Sustainable Energy & Fuels

ROYAL SOCIETY OF CHEMISTRY

PAPER

View Article Online
View Journal | View Issue

Cite this: *Sustainable Energy Fuels*, 2025, **9**, 1217

Poly(diallyldimethylammonium)-based solid electrolytes to significantly enhance the power factor of a thermoelectric oxide film (Sb-doped SnO_2)†

M. Solis-de la Fuente,[a] S. Castro-Ruiz,[a] L. Márquez-García,[a] P. Rullière,[b] S. Fantini,[b] R. Del Olmo,[c] N. Casado[cd] and J. García-Cañadas*[a]

Thermoelectric (TE) materials are able to convert heat into electricity. Suitable TE materials should have high power factors (PFs) and low thermal conductivities, where PF = $S^2\sigma$, with S being the Seebeck coefficient and σ the electrical conductivity. Most recent improvements in TE materials have been achieved by the reduction of the thermal conductivity, and strategies to improve the PF have been minor. Recently, our group reported a new concept to significantly increase the PF, based on the combination of a porous TE solid with an electrolyte. Herein, we made use of this new approach but using polyelectrolytes, rather than the liquid electrolytes previously employed. Poly(diallyldimethylammonium X) polyelectrolytes were tested, where X = Cl^- (C) or tosylate (Tos). An average PF improvement of 2.6 times was obtained when PDADMAC was used, similar to the enhancement with liquid electrolytes. This was due to average decreases of 13% and 71% in the absolute value of the Seebeck coefficient and the electrical resistance of the system, respectively. An electrochemical study by impedance spectroscopy and cyclic voltammetry revealed the better capability of PDADMAC to screen the charge introduced in the oxide compared with that of PDADMATos. The resistance reduction for PDADMAC was attributed to variations in the carrier concentration in the oxide after its equilibration with the polyelectrolyte. The notable PF improvement obtained paves the way for the use of polyelectrolytes to fabricate all-solid-state solid-electrolyte systems with enhanced PFs.

Received 21st October 2024
Accepted 14th January 2025

DOI: 10.1039/d4se01471e

rsc.li/sustainable-energy

Introduction

It is estimated that 72% of the total world energy consumption is currently lost as waste heat,[1] which represents a huge amount of energy. A 10% recovery of this heat energy will exceed the sum of the energy generated by most current renewable energy sources (solar, wind, geothermal, and hydro energies).[2,3] In addition to the waste heat, ubiquitous heat sources such as the sun or even our own bodies are widely available. Under this scenario, technologies able to convert heat into electricity are highly desirable and can enormously contribute to solving the current energy crisis. Thermoelectric (TE) devices are a promising candidate, since they can convert heat into electricity under noiseless, clean, and safe operation.[4,5] This technology has been used in different applications, such as generators in car exhausts, spacecrafts, wood stoves for residential facilities, industrial furnaces, solar power generation, sensors, and self-powered systems, among others.[4–6]

The energy conversion efficiency in a TE material relies on the dimensionless figure of merit $zT = S^2\sigma T/\kappa$, with S being the Seebeck coefficient, σ the electrical conductivity, κ the thermal conductivity, and T the absolute temperature. The product $S^2\sigma$ is known as the power factor (PF). The figure of merit has been significantly improved in the last few decades by mainly reducing the thermal conductivity, typically through nanostructuring or defect engineering. However, κ is now reaching values close to its amorphous limit in many cases, which makes it difficult to achieve further improvements in zT.[7,8] Strategies to increase the PF have been minor and less successful, since they involve decoupling the Seebeck coefficient and the electrical conductivity, which are adversely interrelated.[9–11]

Our group has reported in the past large PF enhancements in a novel solid–liquid TE system, consisting of a porous and nanostructured TE solid material in contact with a liquid electrolyte. Different electrolytes were tested which produced PF improvements when they were brought into contact with

[a]*Department of Industrial Systems Engineering and Design, Universitat Jaume I, Av. Vicent Sos Baynat s/n, 12006 Castelló de la Plana, Spain. E-mail: garciaj@uji.es*
[b]*Solvionic SA, 11 Chemin des Silos, 31100 Toulouse, France*
[c]*POLYMAT, University of the Basque Country UPV/EHU, Joxe Mari Korta Center, 20018 Donostia-San Sebastián, Spain*
[d]*IKERBASQUE, Basque Foundation for Science, 48013 Bilbao, Spain*

† Electronic supplementary information (ESI) available. See DOI: https://doi.org/10.1039/d4se01471e

a nanostructured and porous antimony-doped SnO_2 film. Namely, the use of a lithium tetrafluoroborate ($LiBF_4$) salt dissolved in 3-methoxypropionitrile as an electrolyte led to a 3.4 times PF improvement. In addition, using the ionic liquid 1-butyl-3-methylimidazolium iodide (BMI-I) as an electrolyte provided a 2.4 times PF enhancement.[12] More recently, we have also found a 3.4 times PF improvement using a redox molecule [Cr(III) acetylacetonate] dissolved in 3-methoxypropionitrile as an electrolyte, proving that this system can also be extended to electroactive compounds.[13]

Herein, we aim at evaluating if PF improvements can also be obtained in another type of electrolyte: a solid (gel-like) polyelectrolyte, which, in contrast to liquids, does not experience leakage, sealing or evaporation problems and can produce an all-solid-state device.[14,15]

Poly(diallyldimethylammonium X) (PDADMAX) polyelectrolytes, where X denotes an inorganic anion such as chloride (Cl^-) or tosylate (Tos^-), will be employed. These polyelectrolytes have been used in different areas due to their high ionic conductivity, especially creating novel composites after blending with conjugated polymers.[16] Poly(diallyldimethylammonium chloride) (PDADMAC) is a cationic polymer electrolyte, widely used in industrial applications, mainly as a flocculant in water treatment, even used in potable water due to its low toxicity.[17,18] On the other hand, its high thermal stability (degradation occurs at ~300 °C with a weight loss of ~10%) also makes it suitable for TE applications.[19,20] In fact, a large Seebeck coefficient has been reported ($S \sim 19$ mV K^{-1}) under 70% humidity conditions, although it shows limitations due to its low ionic conductivity.[21] Regarding the Tos^- anions, they have been integrated into poly(3,4-ethylenedioxythiophene) tosylate (PEDOT-Tos) composites to increase the low electrical conductivity of poly(3,4-ethylenedioxythiophene) polystyrene sulfonate (PEDOT-PSS), improving the PF by modulating the oxidation level.[22]

In this article, we analyzed the PF improvements produced when either PDADMAC or PDADMATos was used as the electrolyte in TE solid-electrolyte systems, where the same porous and nanostructured Sb:SnO_2 film previously employed was used as the TE solid. Also, we studied the main mechanisms underlying the results found, using impedance spectroscopy and cyclic voltammetry.

Experimental section

Materials

A commercial Sb:SnO_2 colloidal aqueous dispersion (Keeling & Walker, A20W) was used for the preparation of solid porous films. A poly(diallyldimethylammonium chloride) (PDADMAC) solution (20 wt% in water) was supplied by Solvionic. For PDADMATos preparation, PDADMAC (molecular weight: 400 000–500 000 g mol^{-1}) solution (20 wt% in water) and *p*-toluenesulfonic acid monohydrate (tosylic acid) (98.5%) were acquired from Sigma-Aldrich. Amberlite™ IRN-78 ion exchange resin, OH-form, was obtained from Fisher Scientific. A gallium indium tin (GIT) eutectic alloy was purchased from Alfa Aesar (ref. 14634) and was used as electrical contacts as described below. All chemicals were used as received without further purification.

Sb:SnO_2 film preparation

Nanostructured and porous Sb:SnO_2 films were fabricated using microscope slide glasses of 25 mm × 15 mm size and 1 mm thickness as substrates. These glasses were cleaned and UV-ozone treated following the procedure described elsewhere.[13] Then, a Kapton mask was used covering the glass to leave an area of 10 mm × 5 mm in the center for the deposition of the film. The Sb:SnO_2 colloidal solution was spin coated (Laurell, WS-650MZ) on top of the glasses at 2500 rpm for 15 s. Afterwards, the film was dried at 100 °C for 10 min on a hot plate. Four layers were deposited following this procedure. Then, annealing was performed at 550 °C for 45 min in a furnace (Nabertherm, 400-1) with a 3 °C min^{-1} heating rate. After annealing, platinum electrical contacts were sputtered (Quorum, Q300T D Plus) at the film ends for 1 min. Before the Pt deposition, a chromium seeding layer was sputtered underneath for 15 s to enhance the Pt adherence to the substrate.

PDADMATos preparation

PDADMATos was synthesized *via* a two-step anion exchange reaction, following a previously reported procedure.[23] An aqueous solution of PDADMAC (5 g in 400 mL), which has a similar viscosity to water, was passed through a column filled with the anion exchange resin (Amberlite™ IRN-78) in the hydroxide form. After that, PDADMAOH was neutralized by the dropwise addition of the equimolar aqueous solution of tosylic acid to obtain the required compound using an ice bath for cooling. The obtained solution was stirred at ambient temperature for 12 h. The excess water was then removed by rotatory evaporation under vacuum. The chemical structure of PDADMATos was confirmed by ^{1}H NMR analysis (see Fig. S5†).

Solid-electrolyte system

The PDADMAX polyelectrolytes were deposited at room temperature by drop-casting 10 μL of their solutions on top of the Sb:SnO_2 films avoiding their contact with the Pt contacts. Then, the polyelectrolytes were dried at room temperature overnight. The water content in the polyelectrolytes was monitored by measuring their mass (Ohaus Pioneer balance with ±1 mg precision) at room temperature (50% relative humidity) for 100 h after the addition of polyelectrolyte solution on Sb:SnO_2 films. Fig. 1 shows an image of the solid-electrolyte system and the chemical formula of the polyelectrolytes employed.

The surface morphology and atomic composition of the porous Sb:SnO_2 films, before and after the polyelectrolyte depositions, were obtained by Scanning Electron Microscopy (SEM) using JEOL 7001F equipment from Oxford Instruments with capability for Energy Dispersive X-ray spectroscopy (EDX). X-ray diffraction (XRD) was also performed using a diffractometer (D4 Endeavor from Bruker-AXS) with a Cu Kα radiation source ($\lambda = 1.54056$ Å).

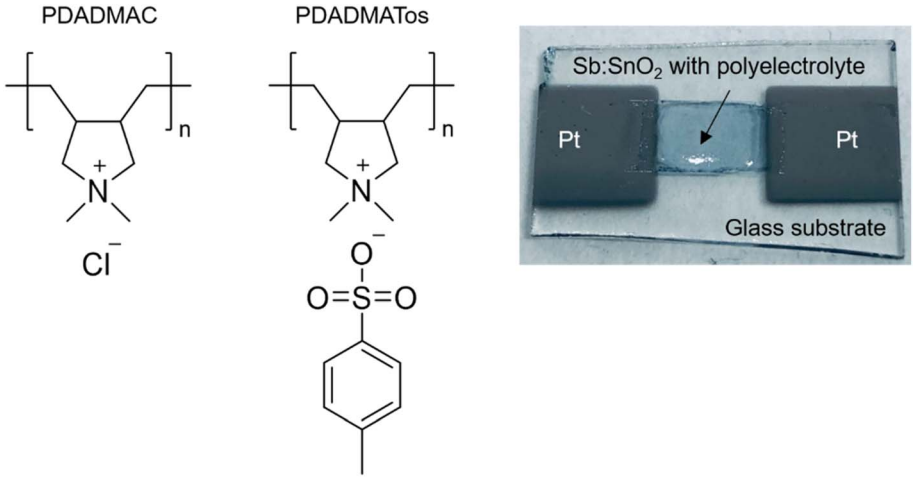

Fig. 1 Chemical formula of PDADMAC and PDADMATos and a photograph of the Sb:SnO_2/PDADMAX system.

TE property measurements

The Seebeck coefficient and electrical resistance of the system were measured using the setup shown in Fig. 2. The heat source consisted of 3 cartridge heaters inserted in a copper block (30 mm × 30 mm x 10 mm) which were powered by a Watlow EZ-ZONE PM temperature controller. On the other hand, a large copper block (50 mm × 50 mm x 30 mm) acted as the heat sink. The cell with the Sb:SnO_2 film and the PDADMAX polyelectrolyte deposited on the glass substrate was placed on top of the copper blocks so that one side lied on the heat source and the other side on the heat sink (see Fig. 2). Thermal grease (RS, ref. 2173835) was used at the glass/copper block interfaces and at the tip of the thermocouples to improve the thermal contacts. Spring probes, held by micropositioners, were used to measure the current and voltage. K-type thermocouples (RS, ref. 8140134) were placed on top of the glass substrate aligned at the ends of the Pt film contacts to measure the temperature difference.

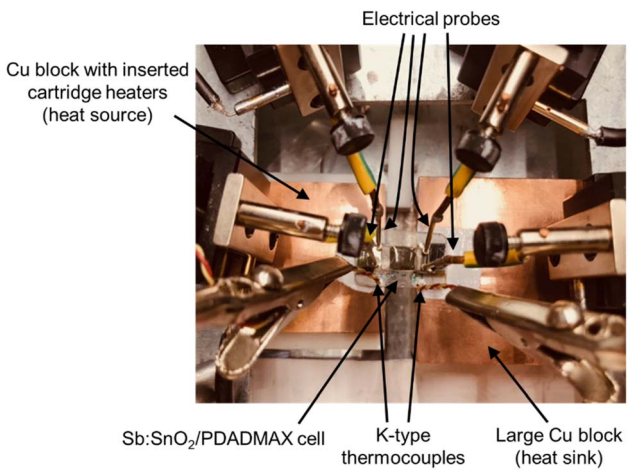

Fig. 2 Top-view photograph of the setup used for thermoelectric measurements.

Electrical resistance was obtained by measuring current–voltage (*I–V*) curves in pseudo-4-probe mode (voltage and current probes contacted at the Pt contacts) at $\Delta T = 5$ K with a Keithley 2450 source meter. In addition, Seebeck coefficient values were obtained from the slope of the open-circuit voltage V_{oc} *vs.* the temperature difference ΔT curve. The temperature was varied from room temperature up to $\Delta T = 5$ K in steps of ~1 K. The V_{oc} was measured using a nanovoltmeter (Keithley 2182A), while the temperature difference was recorded with a dual datalogger thermometer (RS, ref. 1316).

Electrochemical measurements

Impedance spectroscopy and cyclic voltammetry measurements were performed employing a Metrohm Autolab PGSTAT204 instrument, equipped with a FRA32M frequency response analyzer. Potentiostatic impedance spectroscopy measurements were carried out using 0 V as the DC potential and 5 mV as the AC amplitude, with a frequency range of 1 Hz–10 mHz. For these impedance measurements, the probes were contacted in the same way as described for the *I–V* curves above and under a $\Delta T = 5$ K. The connections used for the cyclic voltammetry experiments are indicated below in the next section.

Results and discussion

The structure of the porous Sb:SnO_2 film was identified by X-ray diffraction (see Fig. 3). The XRD spectrum shows diffraction peaks in agreement with the tetragonal structure of cassiterite SnO_2 (R040017, RRUFF Database). Furthermore, elemental composition EDX analysis corroborated the presence of antimony in the structure (see Table S1 and Fig. S1†).

The SEM images of Sb:SnO_2 films before and after the addition of PDAMAC or PDADMATos are shown in Fig. 4. Nanoparticle sizes between 6 and 10 nm and pore dimensions between 2 and 50 nm can be observed in the image (see Fig. 4a). The film thickness was ~1 μm, measured from the cross-sectional view image (see Fig. 4b). The complete penetration

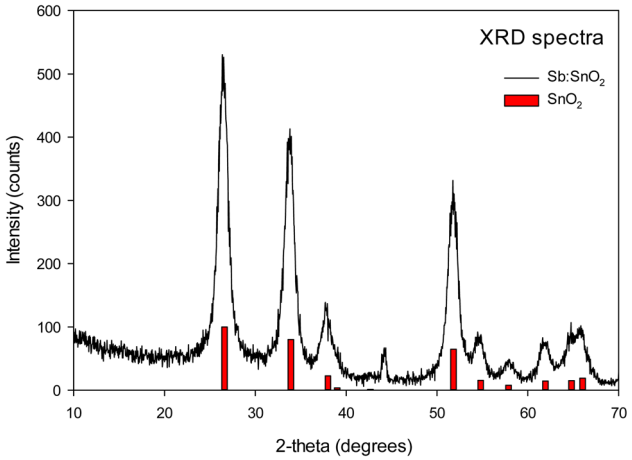

Fig. 3 X-ray diffraction pattern of the $Sb:SnO_2$ film.

of both polyelectrolytes in the porous nanoparticle network of the $Sb:SnO_2$ film is clearly shown in Fig. 4c and d.

Table 1 shows the Seebeck coefficient and electrical resistance values measured for three different $Sb:SnO_2$ films before and after PDAMAC or PDADMATos deposition. The table also shows the PF improvement, determined by the ratio between the PF after and before the polyelectrolyte addition. For the PDADMAC systems, it can be observed that there is a small reduction (13% average) in the absolute value of the Seebeck coefficient and a significant reduction (71% average) in the electrical resistance, leading to a remarkable average PF improvement of 2.6 times, which is similar to the values reported for liquid electrolytes in these systems.[12,13] To prove that the reduction in the electrical resistance is not due to electronic conduction through PDAMAC, the electrical resistance was also

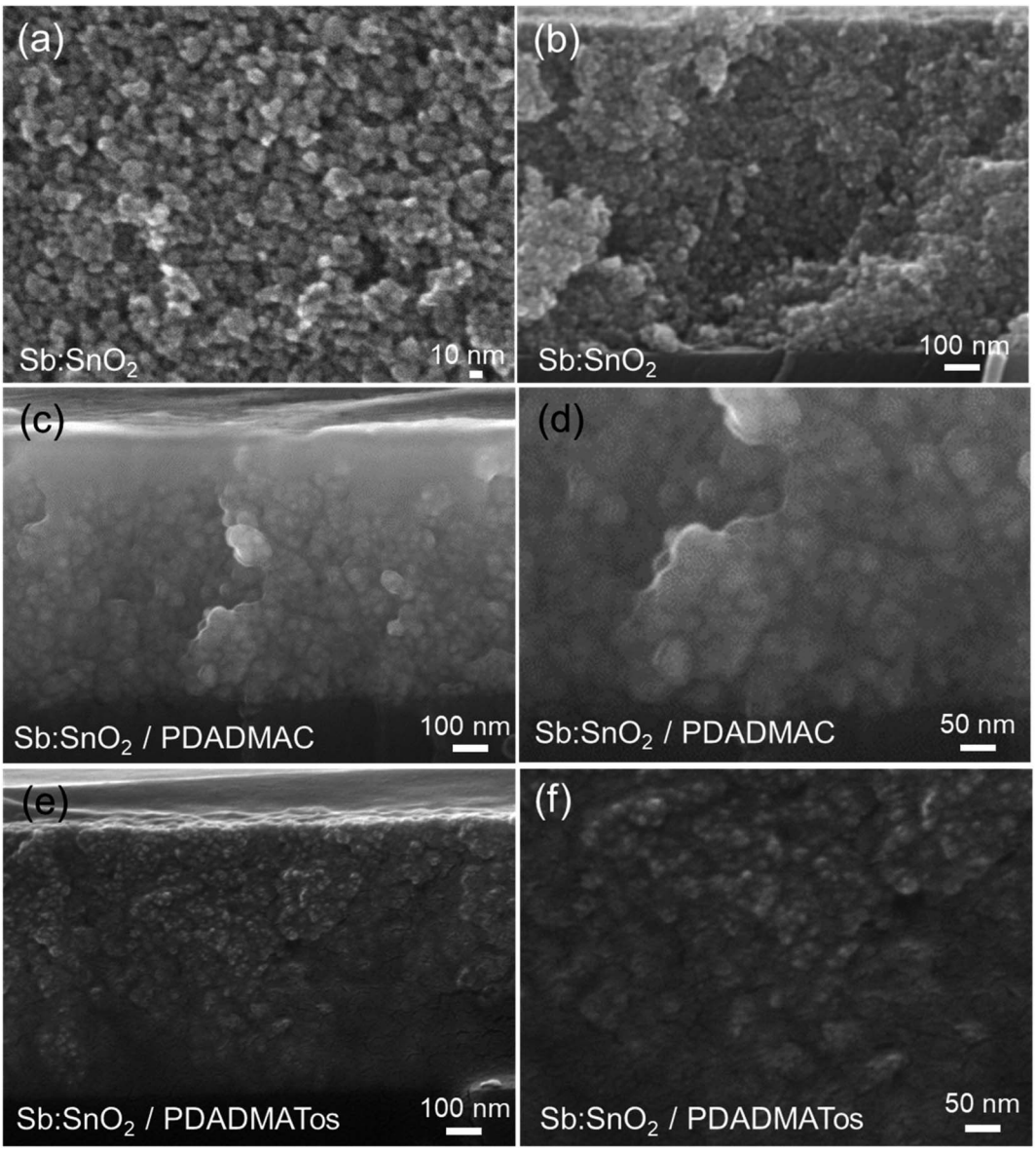

Fig. 4 (a) Top and (b) cross-sectional SEM images of an $Sb:SnO_2$ film without polyelectrolyte added. Cross-sectional SEM images of $Sb:SnO_2$ films after addition of (c and d) PDADMAC and (e and f) PDADMATos.

Table 1 Seebeck coefficient and electrical resistance for Sb:SnO_2 films before and after PDADMAX deposition. Also, the PF ratio after and before the addition of the polyelectrolytes is shown. The temperatures given correspond to the ambient temperatures. Errors were obtained from the linear fittings

	Seebeck coefficient ($\mu V\ K^{-1}$)			Electrical resistance (kΩ)			
	Sb:SnO_2	Sb:SnO_2/PDADMAX	Variation (%)	Sb:SnO_2	Sb:SnO_2/PDADMAX	Variation (%)	PF_{after}/PF_{before}
1-PDADMAC	-41.3 ± 0.22 (17.6 °C)	-36.1 ± 0.31 (19.6 °C)	−12.5	15.0 ± 0.05 (22.6 °C)	4.12 ± 0.02 (24.6 °C)	−72.6	2.80
2-PDADMAC	-46.7 ± 0.51 (18.8 °C)	-39.5 ± 0.40 (16.9 °C)	−15.3	15.1 ± 0.25 (23.8 °C)	4.51 ± 0.08 (21.9 °C)	−70.2	2.41
3-PDADMAC	-51.9 ± 0.82 (18.7 °C)	-45.6 ± 0.33 (17.9 °C)	−12.2	15.7 ± 0.12 (23.6 °C)	4.74 ± 0.05 (22.9 °C)	−69.8	2.56
No Sb:SnO_2	—	—	—	—	5500 (23.4 °C)	—	—
1-PDADMATos	-44.8 ± 0.71 (19.2 °C)	-43.5 ± 0.40 (17.7 °C)	−2.45	19.5 ± 0.34 (24.1 °C)	40.3 ± 0.34 (22.7 °C)	106	0.46
2-PDADMATos	-45.9 ± 0.37 (19.2 °C)	-43.2 ± 0.33 (18.4 °C)	−6.07	10.1 ± 0.03 (24.2 °C)	16.5 ± 0.34 (23.4 °C)	64.0	0.54
3-PDADMATos	-43.9 ± 0.65 (19.3 °C)	-44.1 ± 0.27 (16.9 °C)	0.45	16.6 ± 0.16 (24.3 °C)	32.2 ± 0.66 (21.9 °C)	94.3	0.52

measured for a sample without Sb:SnO_2 (only PDADMAC with the Pt contacts), obtaining a value of 5.5 MΩ, which is several orders of magnitude higher than that of the systems with Sb:SnO_2 (see Table 1, 'No Sb:SnO_2'). In contrast to the PDADMAC results, the systems with PDADMATos produced nearly no variation in the absolute value of Seebeck coefficient (3% average reduction) and a substantial increase (88% average) in the electrical resistance, which led to no PF enhancement. Hence, the presence of Cl^- in the polyelectrolyte is crucial to achieve PF improvements.

It should be noticed that, although the ambient temperature was not constant throughout the measurements in Table 1, the largest variation found between experiments before and after the polyelectrolyte addition is 2.4 °C, which is not high enough to produce the large variations found. In addition, we have reported before that very small changes in both properties (Seebeck coefficient and electrical resistance) occur with temperature (see Fig. S4† of ref. 13).

Although the aim of this study is to identify PF improvements using polyelectrolytes, and with the oxide selected to prove this, not very high PF values are expected, since the initial Seebeck coefficient value of Sb:SnO_2 is modest (~45 $\mu V\ K^{-1}$), we would like to provide an indication of the initial PF value for a meaningful comparison with other TE materials and approaches. To reach the PF, the electrical conductivity can be calculated using the resistance value of the film from Table 1 (~15 kΩ) and the film dimensions given (~1 μm thickness, 10 mm length and 5 mm width), obtaining a value of ~130 S m^{-1} and hence a PF = 0.26 $\mu W\ (K^2\ m)^{-1}$.

In order to understand the effects observed, impedance spectroscopy measurements were performed under operating conditions ($\Delta T = 5$ K) for the 1-PDADMAC and 1-PDADMATos systems of Table 1 (see Fig. 5). The impedance spectra show points lying around certain real impedance (Z') values in all cases, except when PDADMAC is added, this feature being an indication of ohmic behavior (current flows through the film). It should be noticed that these Z' values match well with the electrical resistance results in Table 1. For the Sb:SnO_2/PDADMAC system (blue points), an initial 45° linear trend that closes forming a semicircle is observed. We attribute this response to the accumulation and diffusion of electrons in the film and their screening by PDADMAC ions (chemical capacitance). This is something that frequently occurs in nanostructured and porous metal oxides permeated by electrolytes.[24,25]

When the voltage is decreased by the AC voltage oscillation during the impedance experiment, at one contact, electrons accumulate in the film at the position close to this contact and are screened by PDADMAC ions. This creates a gradient in the electronic concentration and thus electrons diffuse towards the interior of the film. The opposite takes place at the other contact (electronic concentration is reduced by the voltage increase), and electrons diffuse towards this contact. Diffusion takes place semi-infinitely (45° linear part) until the diffusion fluxes from both contacts meet at the half length of the film, where the carrier concentration does not change, since electrons coming from one side are removed at the same rate by the diffusive flux towards the other electrode. Thus, the impedance response

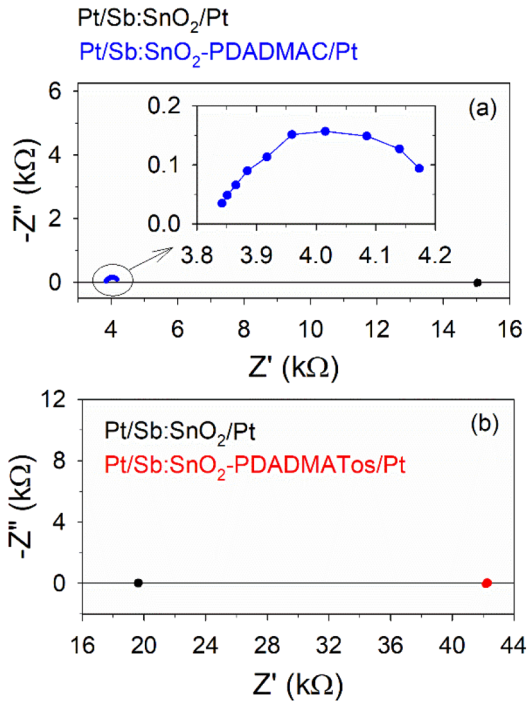

Fig. 5 Impedance spectroscopy carried out at $\Delta T = 5$ K for the Sb:SnO_2 film before and after the deposition of (a) PDADMAC (sample 1-PDADMAC) and (b) PDADMATos (sample 1-PDADMATos).

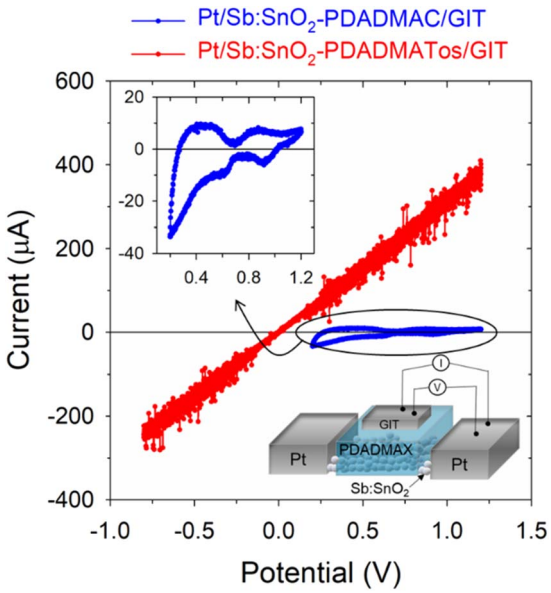

Fig. 6 Cyclic voltammetry experiments at 5 mV s^{-1} for Sb:SnO_2 films with PDADMAC (blue) and PDADMATos (red) polyelectrolytes added. The inset shows a scheme of the system measured and how the electrical contacts were established.

turns into a semicircle, and when the steady state is reached a linear carrier concentration profile is created.

This electronic diffusion does not occur when PDADMATos is used, since the ions in this electrolyte cannot screen the electrons at the solid/polyelectrolyte interface as effectively as in the PDADMAC case. This can be due to the larger size and more complex chemical structure of the Tos^- anion compared to Cl^- and also to the lower water content absorbed in the polymer, as it will be shown below.

Apart from the impedance spectroscopy analysis, cyclic voltammetry experiments at a 5 mV s^{-1} scan rate were also conducted after the addition of the polyelectrolytes (see Fig. 6). In this case, measurements were performed contacting one of the Pt electrodes and in an area on top of the polyelectrolyte where the GIT alloy was spread (see the inset of Fig. 6). In this way, the current now flows from the Pt contact at the oxide towards the GIT.

In the case of PDADMAC, a capacitive response is observed (see blue dots in Fig. 6), which is common in nanostructured and porous oxides.[26,27] Briefly, when the voltage is negatively scanned, electrons are injected into the oxide film at the same time that are screened by the PDADMAC ions at the solid/electrolyte interface (charging of the capacitor). This produces the negative current increase observed. When the voltage is reversed, the injected electrons are extracted (capacitor discharge), and the current turns positive. This response is in agreement with the impedance spectroscopy results mentioned above. Peaks or shoulders can also appear in the cyclic voltammograms, as observed at around 0.5 and 0.9 V, which typically come from trap or surface states.[27] It can be observed in Fig. 6 that this capacitive response is not displayed for PDADMATos. In contrast, a linear trend appears, in agreement with the impedance response of Fig. 5 for this system (ohmic response).

Since the water content in the PDADMAX polyelectrolytes can influence their charge screening capacity, as previously mentioned, this content was monitored by measuring the polyelectrolyte weight during 100 h (see Fig. S4†). It can be observed that the initial mass significantly dropped during the initial hours and then it remained constant. Table 2 shows the main mass variations detected. PDADMAC retained 2.12 g of water after drying, which is 38.5% of the residual mass. On the other hand, PDADMATos retained 1.24 g of water (24.3% of the residual mass). Hence, PDADMAC is clearly a more hygroscopic polyelectrolyte, which can facilitate the movement of its ions, and hence the charge screening, with respect to PDADMATos, where a lower water content exists.

After all the experiments were performed, the variation of the electrical resistance in the Sb:SnO_2/PDADMAX systems evaluated can be attributed to the variation of the carrier concentration in the oxide after equilibration with the polyelectrolytes. In this equilibration process, the electrochemical potential in the oxide aligns with the electrochemical potential of the electrolyte.[25–27] As a consequence, a double layer is formed at the oxide/polyelectrolyte interface, where the ions in the electrolyte balance the increase/decrease of the electronic concentration in the solid. For PDADMAC, the equilibration is more effective, since the screening of electrons by the PDAMAC anions is much easier, as shown by the impedance and cyclic voltammetry analyses. Then, an increase in the carrier concentration of the oxide and hence a significant decrease in the electrical resistance was observed (see the energy diagram of Fig. S6†). For PDADMATos, the screening is more

Table 2 Mass variations and water content in Sb:SnO_2/PDADMAX systems

Polymer solution	Solution mass (mg)	Dried polymer mass (mg)	Residual mass after 24 h of drying (mg)	Calculated mass of residual water (mg)
PDADMAC, 20 wt% in H_2O	16.9	3.38	5.5	2.12
PDADMATos, 20 wt% in H_2O	19.3	3.86	5.1	1.24

complicated, and the equilibration led to a decrease in the carrier concentration.

Conclusions

In this study, the possibility to obtain large improvements in the thermoelectric power factor of a nanostructured and porous oxide (Sb:SbO_2) after being in contact with a solid (gel-like) polyelectrolyte has been evaluated. Two polyelectrolytes with different anions were tested, PDADMAC (with Cl^-) and PDADMATos (with Tos^-). A remarkable average power factor improvement of 2.6 times was found when PDADMAC was used, which is similar to the improvements previously reported for this oxide using liquid electrolytes. The significant improvement was due to a 13% average reduction in the Seebeck coefficient and a 71% average drop in the device electrical resistance. When PDADMATos was used, no power factor improvements were found. Electrochemical analysis by means of impedance spectroscopy and cyclic voltammetry revealed that PDADMAC was able to effectively screen electrons injected into the Sb:SnO_2 film, while PDADMATos did not show this feature. This better screening capability was attributed to the lower size and simpler chemical structure of the Cl^- anion compared to PDADMATos and to the higher water content in PDADMAC. This better screening capability of PDADMAC is identified as an important factor leading to a higher increase in the carrier concentration in the oxide after the equilibration of the electrochemical potentials in both materials (oxide and polyelectrolyte) once they are brought into contact, which is the mechanism described for the reduction of the electrical resistance. This work opens up the possibility to obtain large power factor improvements in thermoelectric oxides when combined with polyelectrolytes and to reach an all-solid-state system, with significant advantages in terms of leakages and sealing with respect to liquid electrolytes. In addition, due to the intricate nanostructured morphology of the thermoelectric material (high number of interfaces/scattering points) and the low thermal conductivity of polymers, low thermal conductivity is expected for these systems, which is also beneficial for the performance.

Data availability

Data for this article are available at Zenodo.

Author contributions

M. Solis-de la Fuente: writing – original draft, visualization, validation, methodology, investigation, formal analysis. S. Castro-Ruiz: writing – review & editing, visualization, validation, methodology, investigation, formal analysis. L. Márquez-García: validation, methodology, investigation. P. Rullière and S. Fantini: methodology, investigation, resources. R. Del Olmo: investigation, writing – review & editing. N. Casado: resources, supervision. J. García-Cañadas: writing – review & editing, visualization, supervision, resources, project administration, methodology, funding acquisition, formal analysis, conceptualization.

Conflicts of interest

There are no conflicts to declare.

Acknowledgements

This project received funding from the European Union's Horizon 2020 research and innovation programme under grant agreement No. 863222 (UncorrelaTEd project). Raquel Oliver and Pepe Ortega are acknowledged for their technical support.

References

1 G. Bianchi, G. P. Panayiotou, L. Aresti, S. A. Kalogirou, G. A. Florides, K. Tsamos, S. A. Tassou and P. Christodoulides, *Energy, Ecol. Environ.*, 2019, **4**, 211–221.
2 C. Forman, I. K. Muritala, R. Pardemann and B. Meyer, *Renewable Sustainable Energy Rev.*, 2016, **57**, 1568–1579.
3 A. Firth, B. Zhang and A. Yang, *Appl. Energy*, 2019, **235**, 1314–1334.
4 D. Beretta, N. Neophytou, J. M. Hodges, M. G. Kanatzidis, D. Narducci, M. Martin-Gonzalez, M. Beekman, B. Balke, G. Cerretti, W. Tremel, A. Zevalkink, A. I. Hofmann, C. Müller, B. Dörling, M. Campoy-Quiles and M. Caironi, *Mater. Sci. Eng., R*, 2019, **138**, 210–255.
5 D. Champier, *Energy Convers. Manage.*, 2017, **140**, 167–181.
6 O. H. Ando Junior, A. L. O. Maran and N. C. Henao, *Renewable Sustainable Energy Rev.*, 2018, **91**, 376–393.
7 Z. Wu, S. Zhang, Z. Liu, E. Mu and Z. Hu, *Nano Energy*, 2022, **91**, 106692.
8 W.-X. Zhou, Y. Cheng, K.-Q. Chen, G. Xie, T. Wang, G. Zhang, W.-X. Zhou, G. Xie, Y. Cheng, G. Zhang, Q. K. Chen and T. Wang, *Adv. Funct. Mater.*, 2020, **30**, 1903829.
9 C. Dun, C. A. Hewitt, H. Huang, J. Xu, C. Zhou, W. Huang, Y. Cui, W. Zhou, Q. Jiang and D. L. Carroll, *Nano Energy*, 2015, **18**, 306–314.
10 A. M. Dehkordi, M. Zebarjadi, J. He and T. M. Tritt, *Mater. Sci. Eng., R*, 2015, **97**, 1–22.
11 Z. Lin, X. Ping, D. Zhao, L. Wang, M. Li, Z. Cai, Y. Zhang, X. Li and X. Zhang, *J. Appl. Phys.*, 2023, **134**, 015101.

12 L. Márquez-García, B. Beltrán-Pitarch, D. Powell, G. Min and J. García-Cañadas, *ACS Appl. Energy Mater.*, 2018, **1**, 254–259.
13 S. Castro-Ruiz, L. Márquez-García, M. Solis-De la Fuente, B. Beltrán-Pitarch, A. Mota-Babiloni, F. Vidan, P. Íñigo-Rabinal, G. Guisado-Barrios and J. García-Cañadas, *Renewable Sustainable Energy Rev.*, 2023, **7**, 4254–4259.
14 J. Duan, B. Yu, L. Huang, B. Hu, M. Xu, G. Feng and J. Zhou, *Joule*, 2021, **5**(4), 768–779.
15 K. S. Ngai, S. Ramesh, K. Ramesh and J. C. Juan, *Ionics*, 2016, **22**(8), 1259–1279.
16 R. Del Olmo, N. Casado, J. L. Olmedo-Martínez, X. Wang and M. Forsyth, *Polymers*, 2020, **12**, 1981.
17 J. Chen, M. Liu, H. Liu, L. Ma, C. Gao, S. Zhu and S. Zhang, *Chem. Eng. J.*, 2010, **159**, 247–256.
18 F. Di Gaudio, S. Barreca and S. Orecchio, *Separations*, 2023, **10**, 311.
19 X. Lyu, B. Clark and A. M. Peterson, *J. Polym. Sci., Part B:Polym. Phys.*, 2017, **55**, 684–691.
20 X. Jia, X. Zhan, J. Xie, B. Gao and Y. Zhang, *J. Macromol. Sci., Part A:Pure Appl. Chem.*, 2019, **57**, 83–90.
21 S. L. Kim, J. H. Hsu and C. Yu, *Org. Electron.*, 2018, **54**, 231–236.
22 O. Bubnova, Z. U. Khan, A. Malti, S. Braun, M. Fahlman, M. Berggren and X. Crispin, *Nat. Mater.*, 2011, **10**(6), 429–433.
23 R. Del Olmo, N. Casado, J. L. Olmedo-Martínez, X. Wang and M. Forsyth, *Polymers*, 2020, **12**, 1981.
24 J. Bisquert, *J. Phys. Chem. B*, 2002, **106**, 325–333.
25 J. Bisquert, *Phys. Chem. Chem. Phys.*, 2003, **5**, 5360–5364.
26 F. Fabregat-Santiago, I. Mora-Seró, G. Garcia-Belmonte and J. Bisquert, *J. Phys. Chem. B*, 2003, **107**, 758–768.
27 J. Bisquert, F. Fabregat-Santiago, I. Mora-Seró, G. Garcia-Belmonte, E. M. Barea and E. Palomares, *Inorg. Chim. Acta*, 2008, **361**, 684–698.